International Journal of Modern Physics E
Vol. 32, No. 7 (2023) 2350038 (24 pages)

DOI: 10.1142/S0218301323500386

World Scientific
www.worldscientific.com

Analysis of centrality dependences of pion multiplicity events using their higher moments in relativistic heavy ion collisions

S. Kamel *,§, A. Saber† and N. Abdallah‡

*Physics Department, Faculty of Education,
Ain Shams University,
Cairo 11757, Egypt

†Department of Basic Science,
Faculty of Engineering in Shoubra,
Benha University, Cairo 11629, Egypt

‡Physics Department,
Faculty of Science, Suez University,
El–Suez 43533, Egypt
§sayedks@windowslive.com

Received 25 May 2023
Revised 23 July 2023
Accepted 8 August 2023
Published 16 September 2023

In this study, data on charged-pion production in relativistic oxygen-ion collisions are examined with varying degrees of centrality. Using the multiplicity of producing charged pions, it is proved that there is a relationship between centrality degrees and collision parameters (such as the impact parameter b, target size fragments, N_h and the total charge of projectile spectators, Q). The various order moments of the multiplicity distributions are used in the standard way to investigate the underlying correlations. The evidence suggests that all the pions produced at the various target sizes (N_h-values) correlate. The higher moments are also investigated at various centrality classes decided by the parameter Q. The multiplicity fluctuations, as measured by the variance-to-mean ratio, showed that the multiplicity distributions of produced pions are not Poissonian, regardless of how they were examined using the two parameters N_h and Q-values.

Keywords: Nucleus–nucleus collisions; charged-pion production; projectile fragmentation; multiplicity distributions; various moments.

PACS Number(s): 25.75.−q, 25.70.Mn, 25.70.Pq, 29.40.Rg

1. Introduction

Recent years have seen significant progress in the study of high-energy nuclear collisions in both nuclear and particle physics. According to whether the kinetic energy per nucleon is close to the nucleon's rest mass, just around 1 GeV (relativistic

§Corresponding author.

collisions), or much larger than the nucleon's rest mass (ultra-relativistic collisions), these collisions are typically divided into two different domains: relativistic and ultra-relativistic collisions.[1–3] In search of the new phase of matter known as the Quark–Gluon–Plasma predicted by the various theories, research into these collisions is growing more popular.[4,5] The production of many particles per event during collisions of heavy ions at relativistic energies is one of the primary benefits, as it helps to study each event separately for further observations. As essential tools for understanding the mechanisms of particle production and exploring the QCD (theory of strong interactions) phase transition, event-by-event fluctuations in thermodynamic quantities have been proposed. The variations of experimentally observable quantities, including temperature, particle ratios, mean transverse momenta, and particle multiplicities, are correlated with the thermodynamic characteristics of the system, including specific heat, entropy, chemical potential and matter compressibility.[6]

The initial overlap region of the colliding nuclei is directly related to centrality, making it a crucial parameter in the study of the characteristics of QCD matter. The impact parameter b, which measures the separation between the centers of the two colliding nuclei, gives it geometric definition. As a result, centrality is correlated with the percentage of the geometric cross-section that overlaps. The participant-spectator picture[7,8] is the most used to describe the collision geometry in nucleus–nucleus collisions with energies greater than 1 GeV/A.

The quantity that best describes the system created by heavy-ion collisions is the multiplicity of the produced particles. By adjusting the impact parameter between the two colliding ions, which also alters the size of the collision volume, it is possible to learn more about the particle production in heavy ion collisions. The most significant inelastic channel in relativistic heavy ion collisions is pion production,[9] which is the subject of our attention. The yield of pions in the final state is correlated with the temperature of the reaction zone via the population of intermediate resonances. Consequently, pions are important in the effort to understand the properties of nuclear matter even though they are not related directly to the equation of state (EOS). Additionally, the production of precisely identifiable pions is the predominant production process at Dubna energy (a few GeV/A).[10] In contrast to nucleons, which are merely liberated during collisions, pions must be generated during the collision process, which makes them extremely intriguing. As a result, they may supply direct insight into the fundamental mechanics of the collision process.

In early studies on the pion production mechanism,[11,12] which explored how the cross-section varies with the mass of the target, the pion production cross-sections were parameterized in the form: $\sigma = A_T^n$, where A_T is the mass number of the target. An $A_T^{1/3}$ dependence for pions with laboratory momenta less than 1 GeV/c supports peripheral production, while a dependence on pions with momenta greater than 1 GeV/c suggests that the pions are formed in more central collisions.

The emitted charged pions employed in this study were created in a nuclear emulsion (Em) experiment in which the plates were exposed to ^{16}O ions at an energy

of 3.7A GeV. The distinctive features of the charged pion multiplicity distributions (MDs) obtained in ^{16}O–Em collisions will be used to discuss collision centrality. The currently popular higher moments are much more susceptible to statistical changes and physical effects. The authors of Ref. 13 proposed that experimental measurements be used to evaluate the empirical relevance of higher-order moments. Higher moments include those associated with fluctuations, skewness, and factorial moments. Such information can be obtained using event-by-event analysis. The STAR Collaboration has recently published measurements on the higher-order cumulants and correlation functions of net-proton (proton) MDs up to the fourth order in Au+Au collisions at the collision energy of the RHIC experiment[14–16] while these measurements are extended to the fifth and sixth orders (also known as hyper-orders) and are reported in Refs. 17 and 18. To examine the net-proton cumulants for central and peripheral Au+Au collisions as a function of energy, these collisions are further separated into centrality classes based on their impact parameters. We will also look at the measurements of higher-order moments for the pion MDs produced in different target sizes.

2. Analysis Method

The correlations of the system are all included in the MDs of multiparticle collisions in an integrated form. The moments or generating functions of the random variables, along with their probabilities can describe any MDs. Moments are calculated as derivatives of the generating function at a position that is extremely close to the singularity, making moment analysis a potent and sensitive method for revealing the structure and microscopic details of MDs.[19]

2.1. *Moments and cumulants of a probability distribution*

Consider a random variable X with a real value and its probability density $f(X)$. The nth order moment of X is defined as

$$\mu_n = \langle X^n \rangle = \int_{-\infty}^{\infty} x^n f(x) dx. \tag{1}$$

When this expected value occurs, the moment-generating function of X is

$$M_X(k) = \langle e^{kX} \rangle, \quad k \in \mathrm{R}. \tag{2}$$

This function, also known as the characteristic function, was constructed to allow for the easy determination of all the distribution's moments. Using Eq. (1) in the series expansion of e^{kX}, Eq. (2) can be written as follows[20]:

$$M_X(k) = \sum_{n=1}^{\infty} \mu_n \frac{k^n}{n!}, \quad \text{with } \mu_n = \left. \frac{d^n M_X(k)}{dk^n} \right|_{k=0}. \tag{3}$$

The cumulant-generating function is used to define the cumulants of a random variable $X : K_X(k) = \log(M_X(k)) = \log\langle e^{kX}\rangle$. The Taylor expansion of the cumulant generating function yields the cumulants k_n once more

$$K_X(k) = \sum_{n=1}^{\infty} k_n \frac{k^n}{n!}, \quad \text{with } k_n = \left.\frac{d^n K_X(k)}{dk^n}\right|_{k=0}. \tag{4}$$

The first cumulant represents the expected value (also known as the mean), while the second and third cumulants, respectively, represent the second (variance) and third centered momenta.

2.2. *Factorial moments of MDs*

MDs can be characterized in terms of the probabilities P to generate n particles at energy E or by the moments of these distributions.[21] The formulas below provide the standard Factorial Moments of a MD (P_n)

$$\begin{aligned} F_q &= \langle n(n-1)\dots(n-q+1)\rangle \\ &\equiv \sum_n n(n-1)\dots(n-q+1)P_n. \end{aligned} \tag{5}$$

The relevance of Factorial Moments stems mostly from the fact that they can be obtained from the generating function $G(z)$; theoretically, this is easier to manage than multiplicity itself.[22,23] One has

$$F_q = \left.\frac{d^q G(z)}{dz^q}\right|_{z=1}, \quad G(z) = \sum_n z^n P_n, \tag{6}$$

which one must generalize to continuous or fractional values of q.

The Poisson distribution[24,25]

$$P_n = \frac{1}{n!}\left(\frac{d}{dz}\right)^n G(z)\bigg|_{z=0} = \frac{\langle n\rangle^n e^{-\langle n\rangle}}{n!}, \tag{7}$$

can be obtained by reversing the generating function $G(z)$ in Eq. (6).

As a result, the distribution is wider (narrower) than the Poisson one and F_q is greater (smaller) than unity if the produced particles are correlated (anticorrelated).

To properly normalize P_n, $1 = G(1)$ is necessary, and the average multiplicity is given by

$$\langle n\rangle = \left.\frac{d}{dz} G(z)\right|_{z=1}. \tag{8}$$

The second Mueller correlation parameter, f_2, grows linearly with $\langle n\rangle (= \sum_n n P_n)$, as predicted by the Mueller–Regge approach.[26] This parameter is specified in terms of the moments $\langle n\rangle^q$ as

$$f_2 = \langle n^2\rangle - \langle n\rangle(1 + \langle n\rangle), \quad f_2^{\text{poisson}} = 0. \tag{9}$$

The fluctuations grow in direct proportion to the multiplicity. The normalized standard moments C_q are defined as follows to prevent the fluctuations from naively increasing in multiplicity:

$$C_q = \frac{\langle n^q \rangle}{\langle n \rangle^q}, \quad q = 1, 2, 3, 4, \tag{10}$$

where

$$\langle n^q \rangle = \sum_{2}^{\infty} n^q \left(\frac{\sigma_n}{\sigma_{\text{inel}}} \right),$$

with n standing for the number of particles produced in an event, and $\langle n \rangle$ being the average multiplicity, σ_n denotes the partial cross-section for creating a state of multiplicity n and σ_{inel} denotes the total inelastic cross-section.

Factorial moments are usually not measured.[27] More common are the central moments

$$\mu_1 = \langle n \rangle = M, \tag{11a}$$
$$\mu_2 = \langle n^2 \rangle - \langle n \rangle^2 = \sigma^2, \tag{11b}$$
$$\mu_3 = \langle (n - \langle n \rangle)^3 \rangle, \tag{11c}$$
$$\mu_4 = \langle (n - \langle n \rangle)^4 \rangle \tag{11d}$$

or their derived characteristics: the skewness (defined as the third-order moment normalized to σ^3)

$$S = \frac{\mu_3}{\mu_2^{3/2}} \tag{12}$$

and the kurtosis (defined by the normalized fourth-order moment -3)

$$\kappa = \frac{\mu_4}{\mu_2^2} - 3. \tag{13}$$

Using the above cumulants (moments), one can calculate the variance, σ^2 the skewness, S and kurtosis, K, for experimentally measured charged pion MDs at different centralities in the current study. According to Ref. 28, the errors of these moments are estimated. The significance of these various moments is further discussed in Ref. 19.

3. Experimental Technique

For this study, stacks of the NIKFI-BR-2 emulsion were subjected to a beam of ^{16}O ions with an energy of 3.7A GeV at the Dubna Synchrophastron in Russia. We used an 850056 STEINDORFF microscope to scan the emulsion pellicles using the "along-the-track" scanning method. The experimental methodology is described in greater detail in Refs. 29 and 30. According to the terminology used in the emulsion experiments,[31,32] we closely followed each beam track for 5 cm or until it encountered

emulsion nuclei. According to their ionization range and velocity, the secondary charged particle tracks produced by each collision were divided into the following categories:

(1) Shower (s-) particles are relativistic secondary particles with a single charge and a velocity greater than $0.7c$. These particles primarily consist of pions produced by the interactions, but they also include some fast protons that have not yet interacted. The letter n_s represents their multiplicity.
(2) Gray (g-) particles have an emulsion range of $L \geq 3\,\text{mm}$ and a velocity of $0.3c \leq v \leq 0.7c$. These tracks are mostly caused by protons with kinetic energies of $26 < T < 400\,\text{MeV}$, as well as deuterons, tritons and slow mesons. N_g represents the mul tiplicity of these fast target protons.
(3) Black (b-) particles have a velocity less than $0.3c$ and a range $L < 3\,\text{mm}$, equivalent to a proton with a $T \leq 26\,\text{MeV}$. The majority of these are created by the evaporation of the residual target nucleus. The symbol N_b denotes the abundance of these slow target protons. In each event, the gray and black tracks are referred to as heavily ionizing particles with $v \leq 0.7c$. $N_h (= N_g + N_b)$ denotes their multiplicity.

The separation of events into ensembles of collisions of distinct projectiles with hydrogen (H), light nuclei (CNO) and heavy nuclei (AgBr) is required by an event-by-event analysis. Typically, events with $N_h \leq 1$ are classified as collisions with hydrogen. CNO events are those that produce two to seven heavy tracks. Collisions with heavy nuclei produce $N_h \geq 8$ events, which certainly belong to AgBr collisions. Using a KSM-1 nuclear track measuring microscope,[33] exact angular measurements of the emitted projectile fragments (PFs) and their charges were conducted.

The charges $Z \geq 2$ of individual PFs were found in each event by combining different approaches[34] such as grain, gap and δ-ray densities. References 35 and 36 supply more information on the charged determination of PFs. The total charge of the PFs $Q = \sum N_i Z_i$ was also computed in each event, where N_i denotes the number of fragments with charge Z_i in the events. The quantity Q is a useful experimental parameter for categorizing nucleus–nucleus (A–A) collisions according to their centrality. As the value of Q increases, centrality decreases. For our experimental events, we have estimated the statistical error related to the typical multiplicities of the shower tracks. Based on the sample standard deviation, the errors considered here are estimates.

4. Experimental Results

4.1. *Multiplicity distributions*

For many years, researchers have investigated the MDs of particles produced in relativistic heavy ion collisions because it can serve as a probe of the dynamics

Table 1. Mean values of n_s and N_h for ^{16}O–Em collisions at various energies.

Energy (A GeV)	$\langle n_s \rangle$	$\langle N_h \rangle$	Ref.
2.1	5.9 ± 0.3	9.3 ± 0.6	40
3.7	10.7 ± 0.3	11.2 ± 0.3	Present work
14.6	20.3 ± 0.8	10.4 ± 0.4	40
60	40.7 ± 2.0	9.4 ± 0.5	40
200	57.3 ± 3.1	7.4 ± 0.4	40

involved in the particle creation mechanism. The MDs of the generated hadrons are a fundamental quantity in describing high-energy inelastic collisions. The information regarding multiparticle correlation is contained in the MDs in its integrated form. It is also a broad and sensitive method for probing the dynamics of interactions. Many results on the MDs of shower particles, which are predominantly pions, in nucleus–nucleus collisions utilizing nuclear emulsion track detectors, have been reported.[37–39] Initially, the multiplicity measurements and later analysis were based on 1875 random events assembled from more recent ^{16}O ions at 3.7A GeV data. The experimental average multiplicities of showers, $\langle n_s \rangle$ and heavily ionizing particles, $\langle N_h \rangle$, for ^{16}O–Em collisions at various energies (2.1–200A GeV)[40] are displayed in Table 1. The findings in Table 1 should be underlined as an improvement over the early data (706 events) published by one of our authors in Ref. 40. The dependence of our $\langle n_s \rangle$ and $\langle N_h \rangle$ results on the interaction centrality degrees represented by the value of N_h, as described in Ref. 41, is investigated further in Table 2 for $N_h 8$, $N_h \geq 8$ and $N_h \geq 28$. As a result, as the N_{h-} value increases, so does the average value of n_s, suggesting that the colliding system prefers more central regions.

To reinforce what is extracted in Table 2, we may classify the primary constituent materials present in the emulsion which has effective mass number 70, into three broad target groups based on the heavy tracks (N_h): hydrogen (H), light nuclei (CNO) and heavy nuclei (AgBr), with effective mass numbers 1, 14 and 94, respectively.[42,43] So, the average multiplicities of $\langle n_s \rangle$ and $\langle N_h \rangle$ for the present data emitted in the collisions of ^{16}O ions with H, CNO, AgBr and Em together with the corresponding values for p–Em,[44] ^{12}C–Em,[45] ^{22}Ne–Em (3.3A GeV)[46] and ^{28}Si–Em[45] at the same incident energy are displayed in Table 3.

Table 2. Mean values of n_s and N_h in 3.7A GeV ^{16}O–Em collisions at different centrality degrees (N_h-regions).

N_h-regions	$\langle n_s \rangle$	$\langle N_h \rangle$
$N_h < 8$	7.15 ± 0.25	4.38 ± 0.16
$N_h \geq 8$	16.42 ± 0.57	21.12 ± 0.73
$N_h \geq 28$	24.63 ± 1.61	34.45 ± 2.26

Table 3. Mean values of n_s and N_h for separate groups of events found in 3.7A GeV ^{16}O–Em collisions compared to the corresponding values of p–Em, ^{12}C–Em, ^{22}Ne–Em and ^{28}Si–Em collisions at the same incident energy.

Projectile	Target	$\langle n_s \rangle$	$\langle N_h \rangle$	Ref.
p	H	–	–	44
	CNO ($N_h < 7$)	1.68 ± 0.03	∼ 2.60	
	Em	1.63 ± 0.02	6.53 ± 0.13	
	AgBr ($N_h \geq 7$)	1.55 ± 0.04	∼ 13.12	
^{12}C	H	0.66 ± 0.05	0.40 ± 0.07	45
	CNO	4.80 ± 0.14	2.83 ± 0.12	
	Em	8.50 ± 0.50	9.10 ± 0.40	
	AgBr	10.80 ± 0.19	16.10 ± 0.34	
^{16}O	H	3.60 ± 0.28	0.49 ± 0.04	Present work
	CNO	6.50 ± 0.24	4.38 ± 0.16	
	Em	10.73 ± 0.25	11.23 ± 0.26	
	AgBr	16.42 ± 0.57	17.99 ± 0.62	
^{22}Ne	H	2.10 ± 0.16	0.52 ± 0.03	46
	CNO	4.46 ± 0.37	4.31 ± 0.16	
	Em	9.98 ± 0.35	10.08 ± 0.36	
	AgBr	19.14 ± 0.86	21.43 ± 0.82	
^{28}Si	H	4.77 ± 0.39	0.41 ± 0.03	47
	CNO	7.06 ± 0.38	3.77 ± 0.22	
	Em	12.90 ± 0.40	11.60 ± 0.13	
	AgBr	21.29 ± 0.88	17.39 ± 0.72	

From Tables (1)–(3), the following conclusions can be drawn:

(i) Although as shown in Table 1, $\langle n_s \rangle$ is mostly decided by the energy, Table 2 shows that $\langle n_s \rangle$ is also decided by the size of the target nuclei. For collisions with projectiles of comparable or greater mass than the target nucleus, Dabrowska *et al.*[48] saw a decrease in the number of target fragments with increasing centrality. Due to intranuclear interactions, a considerable number of involved protons from the target nucleus gain enough momentum to become relativistic as the collision becomes more central.

(ii) For a given target in Table 3, while $\langle N_h \rangle$ (target fragments) is unaffected by the incident projectile mass number (A_P), $\langle n_s \rangle$ (produced pions), increases as A_P increases.

(iii) The average multiplicities of $\langle n_s \rangle$ and $\langle N_h \rangle$ in Table 3 for different projectile masses (A_p) at different impact parameters (different target sizes) show that these values increase as N_h increases (decreasing impact parameter), while in the case of p–Em interaction $\langle n_s \rangle$ is quite independent of N_h. According to Ref. 44, there is no noticeable meson formation in the secondary process, and the relativistic particles are ejected with an increase in the impact parameter following scattering.

The examination of charged particle MDs is critical in obtaining preliminary information on the underlying particle creation mechanism, while the correlations supply specifics on the dynamics. Earlier research[49] on the production of pions in nucleus–nucleus collisions at about $E_{\text{lab}} = 1A$ GeV found that pions interact very strongly with surrounding nucleons. Once created, they may be rescattered or reabsorbed. Two variables have a significant impact on the likelihood of pion reabsorption. First, it is determined by the location of the pion. Second, it is determined by the pions' mean free path. In concept, this quantity is decided by pion energy and nuclear density.

In the following, we have investigated the MDs of pion production in nucleus–emulsion collisions using ^{12}C, ^{16}O and ^{28}Si projectiles at incident energy 3.7A GeV as well as ^{22}Ne at incident energy 3.3A GeV.[35] The MDs of the produced pions have been displayed in Figs. 1(a)–1(d) for ^{12}C–Em, ^{16}O–Em, ^{22}Ne–Em and ^{28}Si–Em collisions, respectively. The MDs for all the projectiles examined in Figs. 1(a)–1(d) have been fitted using the well-known Gaussian distribution function, which is depicted by the solid curve. The Gaussian distribution is a statistical probability function with a straightforward and visually appealing physical interpretation. These figures show that the tail of the distribution extends to significantly greater values of n_s. This clearly shows that when projectile energy and mass number of the projectile nucleus increase, more relativistic charged particles (produced pions) are created, confirming the energy-to-mass conversion. This conclusion, as given in Ref. 50, is consistent with our findings.

The mean multiplicity of charged pions is affected by the projectile mass number, as was found in earlier research.[51] A power-law relation of the form $\langle n_s \rangle = aA_P^b$ well described this dependence Accordingly, Fig. 2 illustrates how average multiplicity,

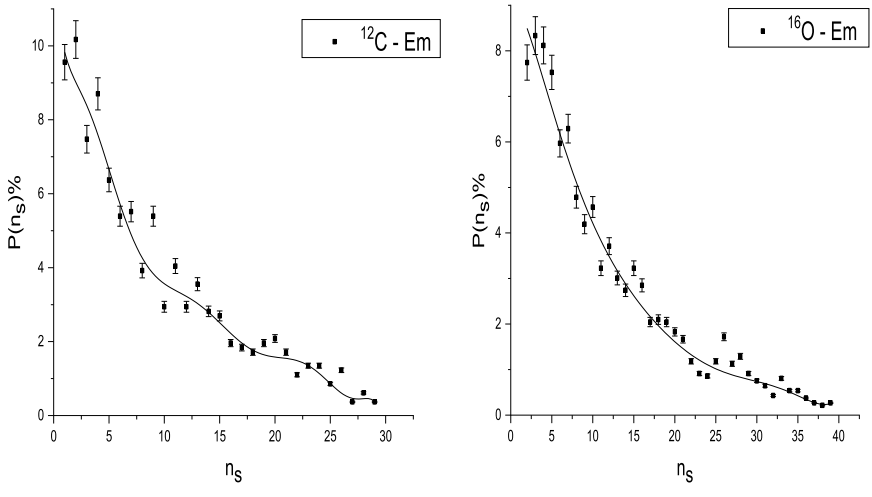

(a) (b)

Fig. 1. (a)–(d) The MDs of pion production, n_s in nucleus–emulsion collisions using ^{12}C, ^{16}O and ^{28}Si projectiles at incident energy 3.7A GeV as well as ^{22}Ne at incident energy 3.3A GeV.

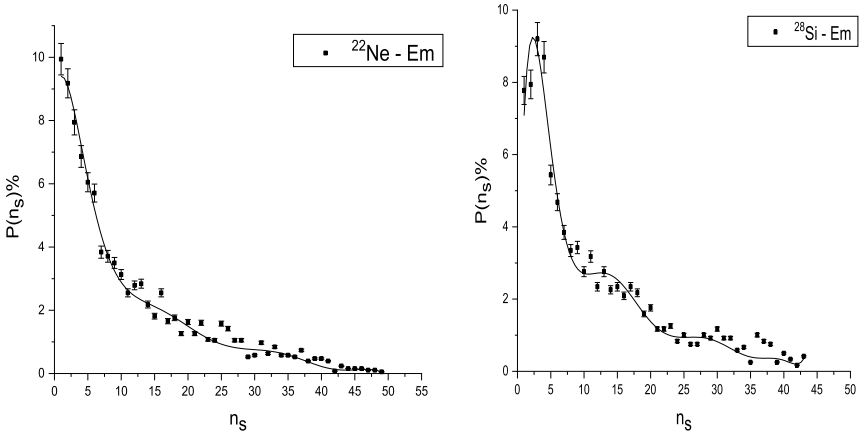

(c) (d)

Fig. 1. (*Continued*)

$\langle n_s \rangle$ using data from Table 3 for emulsion, varies with the mass number A_P. The relation $\langle n_s \rangle = 1.5\ A_P^{0.629}$ has parameterized this variation. This relationship is consistent with what has been published in this regard. It was found that for A_P at an energy of $3.7A$ GeV, the power (slope parameter) is about 0.37 for interactions with CNO target nuclei,[50] 0.5 for interactions with Em target nuclei,[49,53] and 0.66 for interactions with AgBr target nuclei.[52] While this power for A_P with different energies is approximately 0.86.[8] These findings prove that projectile and target mass, as well as incident projectile energy, have an influence on $\langle n_s \rangle$.[54,55]

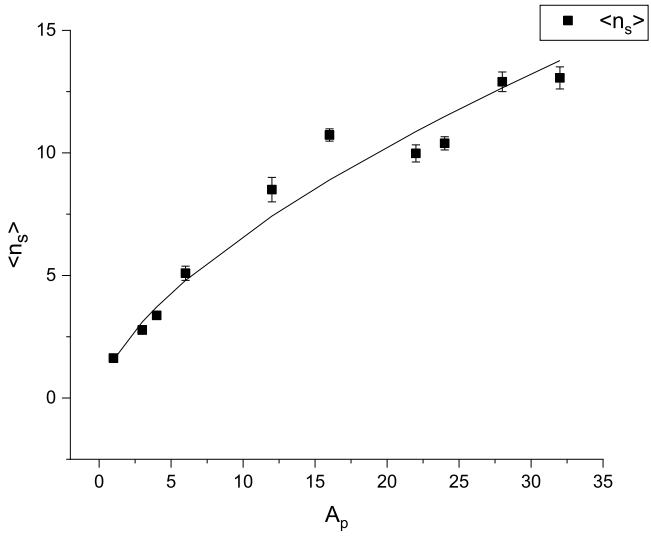

Fig. 2. Variation of $\langle n_s \rangle$ as a function of projectile mass number, A_p.

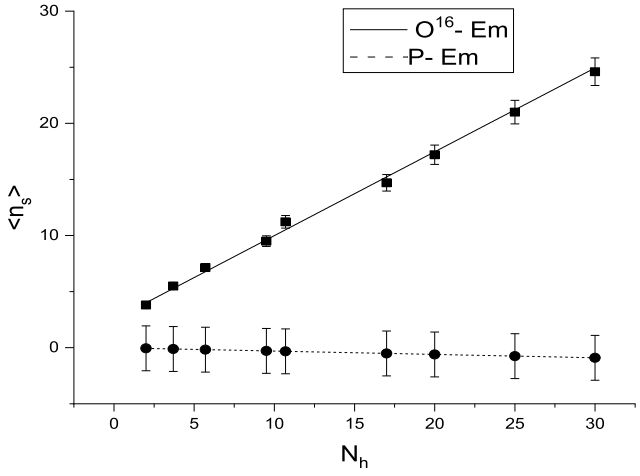

Fig. 3. Dependence of $\langle n_s \rangle$ on N_h in ^{16}O–Em collisions at 3.7 AGeV. Solid line stands for the best fit for the experimental points. Dashed line is the corresponding dependence in p–Em collisions[42] at 3.7 AGeV.

Figure 3 compares the current sample of 3.7A GeV ^{16}O–Em interactions to the 3.7 AGeV p–Em interactions presented in Ref. 44. The dependence of the average multiplicity $\langle n_s \rangle$ on the heavily ionizing particles N_h can be represented by straight lines with a positive slope for ^{16}O–Em and a negative slope for p–Em. The best fits for these linear relationships are $\langle n_s \rangle = 0.72\, N_h \pm 2.66$ for oxygen–emulsion and $\langle n_s \rangle = -0.03\, N_h \pm 2.0$ for proton–emulsion.[44]

As a result, the correlation between $\langle n_s \rangle$ and N_h in ^{16}O–Em interactions is strong and positive, while in p–Em interactions, it is weak and negative.

Information about the collision mechanism may be gleaned from measurements of the total multiplicity of charged particles, their distribution in pseudorapidity space (angular dependence), and their effects on collision centrality and energy. On the other hand, the initial geometry of the strongly interacting matter produced in a heavy-ion collision helps to identify the observables sensitive to its properties.

The initial geometry can theoretically be determined by factors like the impact parameter (b), the quantity of binary nucleon–nucleon collisions ($N_{\rm coll}$) and the quantity of participating nucleons ($N_{\rm part}$).[56] Experimentally, the measured multiplicity of newly created charged particles can be used to define collision geometry. The degree of centrality of an event can be calculated geometrically by knowing the impact parameter b between the centers of two colliding nuclei. This parameter controls the number of interacting nucleons from the projectile and target nuclei. Events with an impact parameter $b = 0$ are known as pure central collisions. Creating selection criteria for central collisions becomes crucial because the impact parameter cannot be measured experimentally in emulsion studies.[57] Heckman *et al.*[58] defined central events as interactions that do not involve projectile fragmentation ($Q = 0$). In emulsion experimental technique, however, the N_h information is typically employed to obtain a sample of central events.[59] The N_h-distribution has been

seen to be energy independent over a wide range of energies in hadron induced (nucleon–nucleus) interactions. Furthermore, N_h was found to be strongly correlated to the centrality of the event. The same is true in recent investigations that use heavy ions as projectiles (nucleus–nucleus interactions).[2,41,46]

Based on the foregoing, the ^{16}O–Em interactions studied in this paper have been grouped into groups of events with varying degrees of centrality. In the first instance, we choose to be this degree by the value of N_h, so that as the interaction becomes more central, the value of N_h grows. As a result, we divided the current data into two major group of events with $2 \leq N_h < 8$ and $N_h \geq 8$. To investigate the centrality of events further, the latter is separated into three subgroups of events: $8 \leq N_h \leq 15$, $16 \leq N_h \leq 27$ and $N_h \geq 28$. The examination of the PFs of the colliding nuclei supplies more information about the collision geometry. However, in the second scenario, we investigate the effect of the impact parameter, which is represented by the value of N_h on Q, which characterizes the volume of the projectile nucleus that is not overlapping the target nucleus. Centrality decreases as the value of Q increases, and vice versa.

As a result, we show the experimental MDs of shower particles, $P(n_s)$, produced in ^{16}O–Em interactions at 3.7A GeV for different centrality groups of events in Figs. 4(a)–4(g). The Gaussian distribution is used to fit the experimental data in this figure. In the first case of $2 \leq N_h < 8$ (peripheral interactions), where the projectile and the target nuclei are far apart and only a minor momentum is transmitted to the interacting nuclei, the production of n_s in Fig. 4(a) decreases with increasing multiplicity. While in the second case of $N_h \geq 8$ (events of ^{16}O–AgBr interactions), $P(n_s)$ in Fig. 4(b), which is represented by a solid curve, increases in its tail.

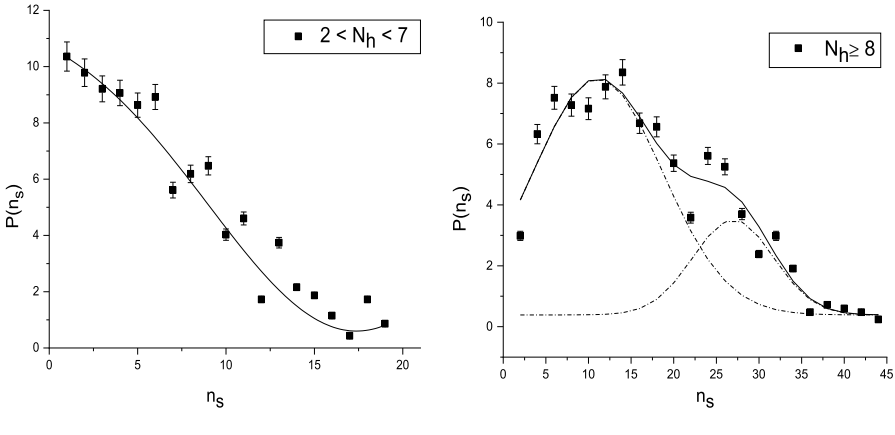

(a) (b)

Fig. 4. MDs of charged pion produced in 3.7A GeV ^{16}O–Em collisions and the corresponding Gaussian distribution for different group of events: (a) $2 \leq N_h < 8$, (b) $N_h \geq 8$, (c) $8 \leq N_h \leq 15$, (d) $16 \leq N_h \leq 27$, (e) $N_h \geq 28$, (f) $Q = 0$ and (g) $N_h \geq 28$ with $Q = 0$.

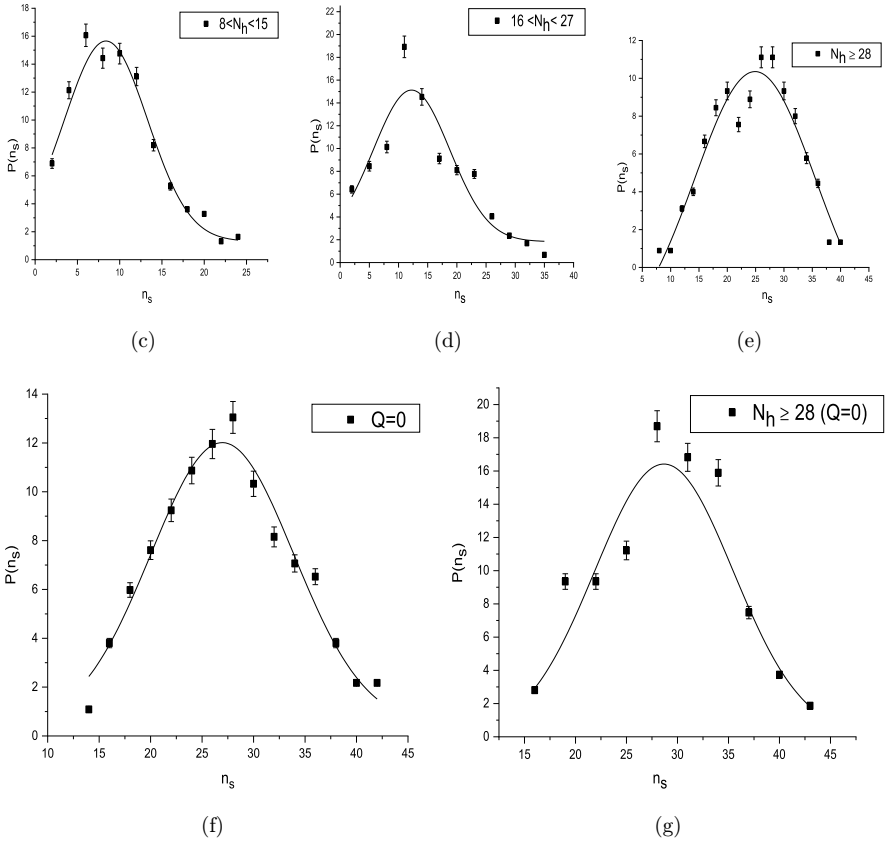

Fig. 4. (*Continued*)

As shown by the dashed curves, this figure may depict contamination of two distributions caused by semi-central and central interactions. This prompts us to examine the centrality degree in the cases of $8 \leq N_h \leq 15$, $16 \leq N_h \leq 27$ and $N_h \geq 28$ in Figs. 4(c)–4(e), where we found the emission of shower particles tends to vary with the target size (that is, with the impact parameter referring to the N_h parameter) and, as previously mentioned, with the parameter Q.

However, it is now possible to investigate the pure central collisions in the last two cases of $Q = 0$ (Fig. 4(f)) and $N_h \geq 28$ with $Q = 0$ (Fig. 4(g)). It is obvious that the central selection criteria of adding the parameter $Q = 0$ to the high degree of target destruction $N_h \geq 28$ is the best. This notion has previously been supported by Ref. 2.

The current charge distribution of the PFs for the entire sample is depicted in Fig. 5. The net charge yield distribution has a J-shaped curve. The most central events (violent collisions) lead the curve to slope downward at first, but semi-central events enable it to begin to rebound, and peripheral events (gentle collisions) cause it to reach a level beyond its starting point. For further analysis, the impact of the

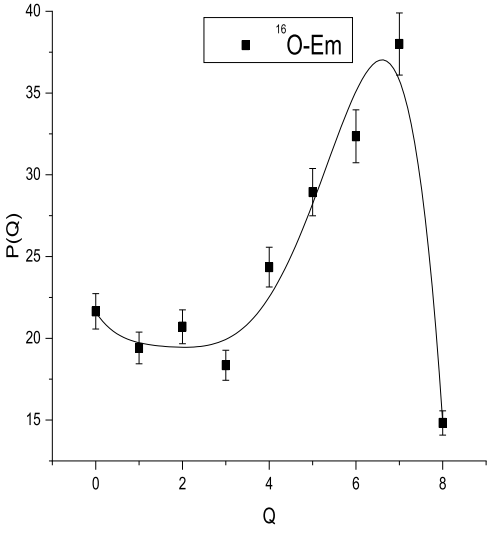

Fig. 5. The yield distribution Q and the corresponding Gaussian distribution for the total sample.

degree of centrality showed by the value of N_h on the total charge of the PF for events with $N_h < 8$, $N_h \geq 8$ and $N_h \geq 28$ is shown in Figs. 6(a)–6(c), respectively. In Fig. 6(a), we observed that in the peripherality of ^{16}O–CNO interactions where $N_h < 8$, the distribution of Q increases until $Q = 6$ and then begins to decrease, showing a link between Q and the gentle low-temperature processes.[60] While in Fig. 6(b), we found that in the weakly and strongly central of ^{16}O–AgBr interactions where $N_h \geq 8$, the charge yield distribution decreases with Q showing the violent-high temperature processes. The strongly central of ^{16}O–AgBr interaction,

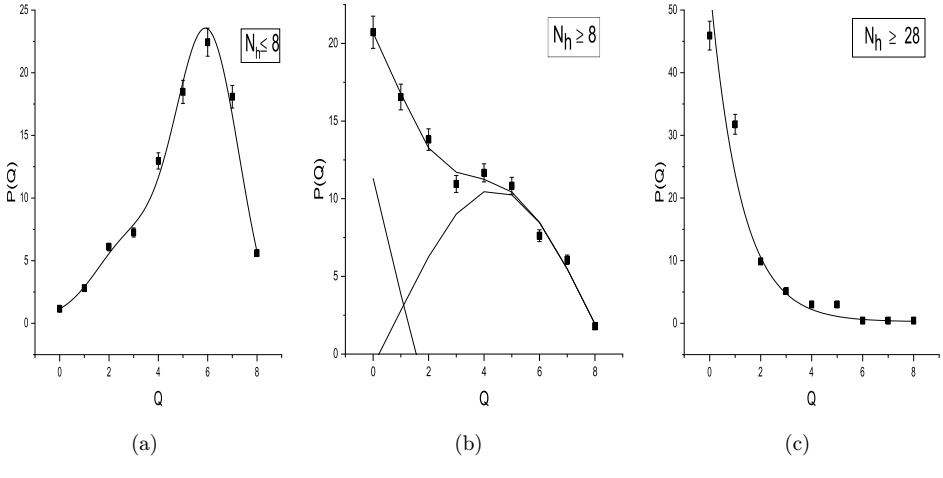

Fig. 6. (a)–(c) The yield distribution Q and the corresponding Gaussian distribution for events having $N_h < 8$, $N_h \geq 8$ and $N_h \geq 28$, respectively.

which confirms the condition of complete overlap of colliding nuclei if $A_{\text{proj.}} << A_{\text{Target}}$,[40] is investigated in Fig. 6(c) for the latter case of $N_h \geq 28$. The exponential decay shape with a maximum value at $Q = 0$ (when all oxygen constituents take part in the collision) is clearly the distinguishing feature of the charge yield distribution.

4.2. *Multiplicity moments of MDs*

To investigate the underlying correlations, the different moments of the MDs (the standard moments, the factorial moments, and the Mueller moments) can be defined in the standard way.[22,61] The fluctuations increase in line with the multiplicity. We can therefore reduce the fluctuation that an irrationally rising multiplicity causes by using the energy–independent reduced moments C_q (Eq. (10)). Table 4 displays the C_q moments with order $q = 2$–5 as well as the second Muller correlation parameter f_2 (Eq. (9)) of the current charged pion particle multiplicity for various event centrality groups. It is obvious that, regardless of N_h groups, all values of C_q increase with q order, while the effect is weak in the last group of events ($N_h \geq 28$ & $(Q = 0)$), or rather, in the last cases characterized by centralization. Multiplicity moments C_3, C_4 and C_5, on the other hand, show a decrease in value as the centrality measured by the N_h parameter increases. It can also be seen that the calculated values of the second Mueller moment, f_2 for all the various groups of events in Table 4 are positive, showing that the shower particles are emitted in a correlated manner.

Higher-order moments[28,62] are much more sensitive to physics effects as well as statistical fluctuations. Beyond the width of the distribution function, the higher moments are more sensitive to its shape. The mean $(M = \langle n_s \rangle)$, variance (s^2), skewness (S) and kurtosis (K) can all be used to characterize unique features of the MDs. These moments are defined in Eqs. (11)–(13), are calculated and tabulated in Table 5 for the shower particle MDs emitted in p–Em,[44] ^{12}C–Em,[37] ^{16}O–Em, ^{22}Ne–Em[44] and ^{28}Si–Em[37] interactions at 3.7A GeV. The mean and variance values are found to increase as the incident mass of the projectile increases. The skewness, S, values calculated for all interactions in Table 5 are all positive, showing that the data are right and highly skewed. Furthermore, apart from the current distribution of ^{16}O–Em, all values of the kurtosis, K, are found to be less than three, indicating that

Table 4. The C_q moments and the second Muller moment, f_2 values of shower particle multiplicity for different centrality groups of N_h in ^{16}O–emulsion collisions at 3.7A GeV.

	C_2	C_3	C_4	C_5	f_2
All N_h	1.57 ± 0.04	3.15 ± 0.07	7.31 ± 0.17	18.45 ± 0.43	62.51 ± 1.44
$N_h < 8$	1.50 ± 0.06	2.88 ± 0.11	6.59 ± 0.25	17.19 ± 0.65	14.92 ± 0.56
$N_h \geq 8$	1.32 ± 0.05	2.07 ± 0.07	3.58 ± 0.12	6.68 ± 0.23	70.61 ± 2.4
$N_h \geq 28$	1.09 ± 0.07	1.25 ± 0.08	1.52 ± 0.10	1.91 ± 0.13	25.49 ± 1.69
$Q = 0$	1.07 ± 0.08	1.22 ± 0.09	1.47 ± 0.11	1.07 ± 0.08	26.94 ± 1.98
$N_h \geq 28$ & $(Q = 0)$	1.06 ± 0.10	1.18 ± 0.88	1.39 ± 0.13	1.72 ± 0.17	20.68 ± 1.99

Table 5. Mean ($= \langle n_s \rangle$), variance (σ^2), skewness (S), kurtosis (K) and scaled variance (ω) for shower particle multiplicity in p–Em, ^{12}C–Em, ^{16}O–Em, ^{22}Ne–Em and ^{28}Si–Em interactions at 3.7A GeV.

Projectile	No of events	M	σ^2	S	K	Excess ($K-3$)	$\omega = \frac{\sigma^2}{M}$	Ref.
P–Em	2576	1.63 ± 0.02	0.96 ± 0.02	—	—	—	0.59	44
^{12}C–Em	819	9.02 ± 0.32	7.16 ± 0.07	0.97 ± 0.09	0.29 ± 0.17	−2.71	0.79	37
^{16}O–Em	1875	10.73 ± 0.25	9.22 ± 0.05	1.51 ± 0.06	4.73 ± 0.11	1.73	0.86	Present work
^{22}Ne–Em	3812	11.61 ± 0.19	10.87 ± 0.04	1.30 ± 0.04	1.10 ± 0.08	−1.90	0.94	37
^{28}Si–Em	1209	12.90 ± 0.37	12.48 ± 0.07	1.47 ± 0.07	1.87 ± 0.14	−1.13	0.97	37

the distributions are platykurtic with shorter and thinner tails, whereas the current distribution with K greater than three is leptokurtic with longer and flatter tails. Increased kurtosis is associated with the probability mass shifting from the distribution's shoulders to its center and tails. The multiplicity fluctuations, on the other hand, have been characterized by the scaled variance (ω) of the MDs, defined as the variance-to-mean ratio, $\left(\frac{\sigma^2}{M}\right)$.[25,61] Multiplicity fluctuations include both statistical (random) and dynamical (deterministic) components.[6] Table 5 also shows the size of the fluctuations, which is quantified in terms of the scaled variance. This table shows that the values of the scaled variance are less than unity, showing that the MDs are narrower than the Poissonian distribution. The shower particles are thus anti-correlated.

Table 6 computes the various order moments for the MDs of shower particles emitted in 3.7A GeV ^{16}O–Em collisions at different target sizes (N_h-values). Table 6 also shows the scaled variance, ω, as well as the mean total charge of the PFs, $\langle Q \rangle$, for each N_h interval. As a result, the target size influences the mean and variance. The data in the peripheral ($2 \leq N_h \leq 7$) and semi-peripheral ($8 \leq N_h \leq 15$) collisions appear to be highly skewed, while the data in semi-central and central collisions appear to be moderately skewed. The excess kurtosis values for all target sizes are negative, showing that the tails of MDs are shorter and thinner than the standard normal distribution. Because the scaled variance values are less than one, the emitted shower particles are anti-correlated. Table 6 also shows that the impact parameter

Table 6. Values of different order moments (M, σ^2, S and K) as well as the scaled variance, ω of n_s MDs and the average total charge of the PFs, $\langle Q \rangle$ at different target sizes (N_h-values) in ^{16}O–Em interactions at 3.7A GeV.

N_h	M	σ^2	S	K	Excess ($K-3$)	$\omega = \frac{\sigma^2}{M}$	$\langle Q \rangle$
2–7	7.15 ± 0.27	5.22 ± 0.06	1.11 ± 0.09	0.70 ± 0.17	−2.30	0.73	5.78
8–15	9.56 ± 0.54	5.90 ± 0.10	1.40 ± 1.38	1.86 ± 0.28	−1.14	0.62	5.01
16–27	17.15 ± 1.00	8.80 ± 0.12	0.59 ± 0.14	0.41 ± 0.28	−2.59	0.51	2.64
≥ 28	24.63 ± 1.61	7.93 ± 0.23	0.32 ± 0.16	0.66 ± 0.32	−2.34	0.32	0.61

influences the mean total charge of the PFs, with $\langle Q \rangle$ decreasing as collision centrality increases.

The analysis of fragments of colliding nuclei provides more information about the collision geometry.[63] Nucleons from interacting nuclei are divided into two groups: those that take part in an inelastic collision with at least one nucleon from the opposing nucleus (participants) and those that do not (spectators). Participants generate secondary particles that are detected by detectors. Nucleon-spectators are nucleon fragments formed by colliding nuclei.[64] The overlap of the interacting nuclei should increase as the total fragment charge decreases. As a result, fragmentation analysis should significantly improve the accuracy of estimating the initial state parameters of the interaction.

In Table 6, we investigated the various order moments at various target sizes (N_h-values). In Table 7, we will examine the various order moments of shower particles emitted in ^{16}O–Em interactions at 3.7A GeV at various centrality classes defined by the parameter Q, the total charge of noninteracting PFs. Table 7 calculates and displays the values of various moments (M, σ^2, S and K), scaled variance ($\omega = \sigma^2/M$) and $\langle N_h \rangle$. Table 7 also shows the current total $\langle n_s \rangle$ in ^{16}O–Em collisions in comparison to $\langle n_s \rangle$ in p–Em (defined as $R = M/1.63$) at the same incident energy, as well as the calculated average number of interacting nucleons defined as $\langle N_{\text{int}} \rangle = A - \frac{A}{Z} Q$ $(= 16 - 2\ Q)$ for the current projectile nucleus.[65]

From Table 7, we can deduce the following:

(1) In general, the first ($M = \langle n_s \rangle$) and second (σ^2) moments of shower MDs as well as the mean of heavily ionizing particles ($\langle N_h \rangle$) increase as the degree of centrality of the collisions increases (that is, for collisions with a lower Q-value).
(2) The degree of centrality has a significant effect on both the mean number of interacting nucleons ($\langle N_{\text{int}} \rangle$) and the ratio R $(= M/1.63)$, lending support to the theory of superposition on nucleons. Furthermore, the participant model, which treats nucleus–nucleus collisions as superpositions of nucleon–nucleon interactions, can be used to estimate the multiplicity fluctuation described in Ref. 66.
(3) The variance equals the mean value for the Poissonian distribution. As a result, the measured scaled variance, ω of the MDs, which measure the multiplicity fluctuations, is not a Poissonian distribution. The scaled variance and Q-values appear to have a positive monotonic relationship.
(4) The distributions for the most central collision events (with $Q = 0$) and semi-central collision events (with $Q = 1$) in the final state are right-skewed and thus the distributions are moderately skewed. Whereas the values of kurtosis in both cases are less than three, showing that the datasets have lighter tails than a normal distribution, the distributions are platykurtic, with shorter and thinner tails.
(5) The distributions for the semi-central collisions (with $Q = 2$ and 3) are also right skewed and seem to be moderately skewed ($S \approx +1$). Whereas the kurtosis values are more than three, showing that the distributions are leptokurtic with longer and fatter tails. Because of its low frequency, the case of $Q = 4$ is ignored.

Table 7. Values of various order moments (M, σ^2, S and K), scaled variance, $\langle N_h \rangle$, R ($= M/1.63$) and $\langle N_{\rm int} \rangle$ in various centrality classes characterized by the parameter Q in ^{16}O–E$_m$ interactions at 3.7A GeV.

Q-value	0	1	2	3	4	5	6	7	8
M	26.90 ± 1.98	21.40 ± 1.66	16.44 ± 1.24	12.89 ± 1.03	10.35 ± 0.72	7.20 ± 0.46	5.09 ± 0.30	3.20 ± 0.18	2.48 ± 0.22
σ^2	7.41 ± 0.28	7.50 ± 0.15	5.67 ± 0.13	5.42 ± 0.13	3.95 ± 0.97	3.68 ± 0.09	2.81 ± 0.07	2.40 ± 0.06	1.46 ± 0.08
S	0.40 ± 0.14	0.56 ± 0.19	1.08 ± 0.18	1.16 ± 0.20	0.40 ± 0.17	1.72 ± 0.16	1.52 ± 0.15	2.81 ± 0.14	2.24 ± 0.22
K	0.13 ± 0.30	0.57 ± 0.38	3.57 ± 0.37	4.05 ± 0.39	0.06 ± 0.34	6.50 ± 0.31	6.41 ± 0.30	4.32 ± 0.27	5.05 ± 0.44
σ^2/M	0.28	0.35	0.35	0.42	0.38	0.51	0.56	0.75	0.55
$\langle N_h \rangle$	28.97 ± 2.14	23.26 ± 1.81	14.83 ± 1.12	12.48 ±0.10	9.77 ± 0.68	7.73 ± 0.49	5.30 ± 0.32	4.46 ± 0.25	3.15 ± 0.28
$\frac{M}{1.63}$	16.50	13.13	10.09	7.91	6.35	4.42	3.12	1.96	1.52
$\langle N_{\rm int} \rangle$	16	14	12	10	8	6	4	2	0

(6) The distributions for the semi-peripheral collisions (with $Q = 5$ and 6) and peripheral once (with $Q = 7$ and 8) are both positively and highly skewed ($S > +1$). Whereas the kurtosis values in both cases are larger than three, showing that the tails of distributions become heavier than a normal distribution.

5. Statistical and Systematic Uncertainties

Systematic errors can be brought on by the scanning process, the fading of tracks, the nuclear emulsion's insensitivity, the existence of background tracks, the detection of PFs, and shower particles. These are the causes of the systematic errors in nuclear emulsion detectors.[67]

The majority of interactions were located using the "along-the-track" scanning technique because of its high detection effectiveness and the fact that it offers reliable event samples. In the forward direction, the scanning was done swiftly, and in the reverse direction, slowly. Two different observers looked at each plate in order to minimize biases in the detection, counting, and measurement processes. According to this approach, we can achieve a scanning efficiency of more than 99%. As a result, less than 1% of the systematic uncertainties are attributable to the scanning and measurement processes.

In order to increase the effectiveness of detecting nuclear emulsion tracks, Alexandrov *et al.* conducted a study.[68] In the current experiment, the emulsion stacks' development caused an average shrinkage factor of 2.2. By evaluating the grain density of the minimum ionizing particle track, the plates' sensitivity is evaluated. Its measurement yields an average value of 28 grains per 100 mm.

The majority of the shower's particles (more than 90%) are pions[31,32,69] with kinetic energies (KE) greater than 70 MeV. They move with a relative velocity of $\beta \geq 0.7$. According to the findings of Adamovich *et al.*, pions are thought to make up the majority of generated particles.[69] They view the shower's particles as pions. Protons, baryons and K-mesons have a contamination of no more than 10% at most. The projectile beam, target nucleus and incident energy all have an impact on the extent of contamination brought on by the presence of kaons and hyperons.

The inability of the nuclear emulsion track detector to distinguish between pions and other mesons or hyperons is another source of systematic uncertainty.[70] Although the shower particles can balance out the pion generation mechanism's dominance, we cannot assert that they offer an accurate evaluation of pions. According to statisticians, the acceptable range for a precise comparison is often set at ± 2 standard deviations, much like in a traditional laboratory experiment. The systematic uncertainty in this work does not reach this top limit of standard deviations.

6. Summary

In summary, almost all the energy in $A - A$ collisions at relativistic energies is deposited in the central region, or the area where two colliding nuclei overlap. This

region is ultimately responsible for the multiple production of newly created particles. As a result, we investigated the characteristics of multiplicity charged-pions produced in $3.7A$ GeV ^{16}O–Em collisions with varying degrees of centrality. To investigate the connection between collision geometry parameters and centrality degree, we used the two parameters of the target size fragments, N_h and total charge PFs, Q. The experimental results of the mean values of n_s and N_h were compared with different prior findings concerning different energies, projectile masses and target sizes. For each specified centrality, the various order moments of the charged pion MD including mean, σ^2, S and K, which are more sensitive to the shape of the distribution, as well as the C-moments, are calculated. On the other hand, these various moments as well as the scaled variance of the current results were compared with other experimental data for different projectile masses having the same incident energy. Let us now summarize our findings.

(1) The projectile mass number, incident energy, and size of the target nuclei all have an impact on the mean multiplicity of produced charged pions.
(2) When the parameter N_h is present, the values of $\langle n_s \rangle$ and $\langle N_h \rangle$ for different nucleus–Em collisions increase with decreasing the impact parameter, and we found that $\langle n_s \rangle$ and N_h have a strong positive correlation in the current ^{16}O–Em interactions. In contrast to nucleon–Em collisions, where $\langle n_s \rangle$ is completely independent of N_h, p–Em interactions are observed to have a weak and negative correlation, which may be due to the lack of detectable meson formation in the secondary process.[42]
(3) The MDs of charged pions produced in each of the projectile collisions that were studied (^{12}C–Em, ^{16}O–Em, ^{28}Si–Em and ^{22}Ne–Em collisions) have been well fitted with the Gaussian distribution function, displaying a tail that extends to noticeably higher values of n_s.
(4) In nucleus–emulsion collisions, the mean multiplicity increases with projectile mass according to a power law relationship of the form $\langle n_s \rangle = 1.5\ A_P^{0.629}$, with this power varying with target size (i.e., CNO or AgBr).
(5) By classifying the ^{16}O–Em collisions into groups of events with various degrees of centrality based on the collision geometry, we investigated the centrality of the events using the parameters N_h, Q, or both. And we found that (i) in peripheral collisions (CNO-events), the production of n_s declines with increasing multiplicity in a decay-shaped curve suggesting a system of production from a single source. Whereas in central collisions (AgBr-events), the MD, which may represent the contamination of two distributions brought on by semi-central and central collisions, grows in its tail; (ii) the best investigation of the pure central selection criteria is thought to be one that adds events with $Q = 0$ to events with a high degree of target destruction and $N_h \geq 28$.
(6) The measured values of C_q moments rise with q order regardless of N_h groups, though the effect is less pronounced in situations where centralization is the case. As the N_h parameter rises, the multiplicity moments (C_3, C_4 and C_5)

show a decline in value. Additionally, in the current experiment, the second Muller moment, f_2, which is nonzero, shows that the charged pions produce in a correlated manner.

(7) As the incident mass of the projectile rises, we found that the mean and variance values rise as well. Consequently, all the examined interactions have values of scaled variance (also known as relative fluctuation) that are less than unity, proving the anti-correlation of the produced pions, and their narrower distribution than the Poisson one. Additionally, we noticed that the scaled variances decreased as the centrality degree increased. Thus, the multiplicity fluctuations of the produced pions have been found to closely match the outcomes of the direct participant model.[51]

(8) Due to the positive skewness that was measured for the MDs of produced pions, the asymmetric shape in each of the examined interactions is skewed to the right in relation to the mean position of the normal distribution. When taking the centrality degree into account using the N_h-parameter in the current interaction, we observed that the target size has an impact on the skewness value, where it changes from being highly skewed in the peripherality cases to being middling skewed in the centrality ones.

(9) Kurtosis, which means varying variance, is the ideal quantity when analyzing the non-Gaussian fluctuation characteristic. Although the values of excess kurtosis are all negative when considering the change in centrality degree, the excess K-values of the current distribution of the entire sample is positive, showing that the MDs are leptokurtic with longer and flatter tails. The excess K-values for the other distributions investigated are negative, referring to platykurtic distributions with shorter and thinner tails.

(10) Our analysis of the higher-order moments at various centrality classes, as decided by parameter Q, revealed that while the first and second moments increased with the degree of centrality, the relative fluctuation decreased. Furthermore, the centrality degree influences both the mean number of interacting nucleons ($= 16–2Q$) and the ratio R ($= \langle n_s \rangle_{\mathrm{O-Em}} / \langle n_s \rangle_{\mathrm{p-Em}}$), supporting the theory of superposition on nucleons.

(11) The investigation of the skewness of the charged-pion MDs in different centrality classes, as decided by the Q-values, shows that the distribution is reasonably skewed in the central collisions (at low Q-values), then becomes highly skewed in the peripheral ones (at high Q-values). In contrast, kurtosis value analysis shows that the distributions' tails are lighter at low Q-values and heavier at high Q-values when compared to a normal distribution.

Recently, physics findings for a certain event centrality class have been addressed in Ref. 18. Understanding the correlation between the experimentally measured reference multiplicity distribution and the extracted class of collision centrality is crucial because the physics of higher-order cumulants and their ratios are thought to be sensitive to collision dynamics, including collision centrality. It is generally known

that, particularly at low-energy collisions, quantum fluctuations in particle creation and fluctuations of the involved nucleon pairs will have an impact on the ultimate centrality determination.

Acknowledgments

We performed this work in the Mohamed El-Nadi High Energy Laboratory, Department of Physics, Faculty of Science, Cairo University, Cairo, Egypt. The authors want to thank all (Vekseler and Baldin) High Energy Laboratory in JINR, Dubna, Russia, for providing us with the irradiated emulsion plates at Synchrophasotron.

ORCID

S. Kamel https://orcid.org/0000-0003-4606-8038

References

1. S. S. Ali and H. Khushnood, *Eur. Phys. Lett.* **65** (2004) 773, https://doi.org/10.1209/epl/i2002-10003-3
2. M. El-Nadi *et al.*, *Eur. Phys. J. A* **10** (2001) 177, https://doi.org/10.1007/s100500170130
3. N. Marimuthu, V. Singh and S. S. R. Inbanathan, *Adv. High Energy Phys.* **2017** (2017) 7907858, https://doi.org/10.1155/2017/7907858
4. F. Paerels *et al.*, arXiv:0904.0435v1 [astro-ph. HE].
5. S. K. Tiwari and C. P. Singh, *Adv. High Energy Phys.* **2013** (2013) 805413, https://doi.org/10.1155/2013/805413
6. M. Mukherjee *et al.*, *J. Phys. G: Nucl. Part. Phys.* **43** (2016) 085102, https://iopscience.iop.org/article/10.1088/0954-3899/43/8/085102
7. S. Nagamiya, *Prog. Part. Nucl. Phys.* **15** (1985) 363.
8. M. K. Singh *et al.*, *Indian J. Phys.* **85** (2011) 1523, https://doi.org/10.1007/s12648-011-0170-z
9. A. Abdelsalam *et al.*, *Int. J. Mod. Phys. E* **27** (2018) 1850026, https://doi.org/10.1142/S021830131850026X
10. M. Anikina *et al.*, *Nucl. Phys. A* **640** (1998) 117, https://doi.org/10.1016/S0375-9474(98)00439-4
11. J. Papp *et al.*, *Phys. Rev. Lett.* **34** (1975) 601, https://doi.org/10.1103/PhysRevLett.34.991.
12. L. S. Schroeder (1980), https://escholarship.org/uc/item/84n7q1c4.
13. STAR Collab. (L. Adamczyk *et al.*), *Phys. Lett. B* **785** (2018) 551, https://doi.org/10.1016/j.physletb.2018.07.066
14. STAR Collab. (J. Adam *et al.*), *Phys. Rev. Lett.* **126** (2021) 092301, https://doi.org/10.1103/PhysRevLett.126.092301
15. STAR Collab. (M. S. Abdallah *et al.*), *Phys. Rev. Lett.* **128** (2022) 202303, https://doi.org/10.1103/PhysRevLett.128.202303
16. STAR Collab. (M. S. Abdallah *et al.*), *Phys. Rev. C* **104** (2021) 024902, https://doi.org/10.1103/PhysRevC.104.024902
17. STAR Collab. (B. E. Abonna *et al.*), *Phys. Rev. Lett.* **130** (2023) 082301, arXiv:2207.09837v2 [nucl-ex].

18. STAR Collab. (M. S. Abdallah *et al.*), *Phys. Rev. C* **107** (2023) 024908, arXiv:2209.11940v2 [nucl-ex].
19. R. S. Bhalerao, *Eur. Phys. J. Spec. Top.* **230** (2021) 635, https://doi.org/10.1140/epjs/s11734-021-00019-x
20. O. Dauchot and V. Démery, *Key Concepts of Statistical Physics* (2017), https://www.pct.espci.fr/∼vdemery/files/KCSP.pdf
21. I. M. Dremin, arXiv:0404092 v1 [hep-ph].
22. A. Capella *et al.*, arXiv:hep-ph/9604247v1.
23. D. Ghosh *et al.*, *Phys. Scr.* **84** (2011) 015201, https://iopscience.iop.org/article/10.1088/0031-8949/84/01/015201.
24. D. Ghosh, A. Deb, S. Bhattacharyya and U. Datta, *Int. J. Mod. Phys. E* **20** (2011) 1171, https://doi.org/10.1142/S0218301311018319.
25. M. Le Bellac, *Acta Phys. Pol. B* **4** (1973) 901.
26. A. H. Mueller, *Phys. Rev. D* **4** (1971) 150, https://doi.org/10.1103/PhysRevD.4.150
27. R. Sochorová, *Phys. Rev. C* **98** (2018) 064907, https://link.aps.org/doi/10.1103/PhysRevC.98.064907
28. X. Luo, *J. Phys. G: Nucl. Part. Phys.* **39** (2012) 025008, https://iopscience.iop.org/article/10.1088/0954-3899/39/2/025008/pdf
29. A. Abdelsalam *et al.*, *J. Phys. G: Nucl. Part. Phys.* **39** (2012) 105104, https://doi.org/10.1088/0954-3899/39/10/105104
30. A. Abdelsalam *et al.*, *Int. J. Mod. Phys. E* **25** (2016) 1650034, https://doi.org/10.1142/S0218301316500348
31. C. F. Powell, F. H. Fowler and D. H. Perkins, *The Study of Elementary Particles by the Photographic Method: An Account of the Principal Techniques and Discoveries Illustrated by an Atlas of Photomicrographs* (Pergamon Press, London, New York, 1959).
32. H. Barkas, *Nuclear Research Emulsion: Technique and Theory*, Vol. 1 (Academic Press, New York, 1963).
33. O. E. Badawy and A. Abd-el-Salam, *Ann. Phys.* **490** (1978) 344, https://doi.org/10.1002/andp.19784900503
34. M. El-Nadi *et al.*, *J. Phys. G: Nucl. Part. Phys.* **24** (1998) 2265, https://doi.org/10.1088/0954-3899/24/12/012
35. M. El-Nadi *et al.*, *Radiat. Meas.* **28** (1997) 231.
36. A. El-Naghy, *Z. Phys. A* **302** (1981) 261, https://doi.org/10.1007/BF01415546
37. M. El-Nadi *et al.*, *Int. J. Mod. Phys. E* **3** (1994) 811, https://doi.org/10.1142/S0218301394000243
38. M. El-Nadi *et al.*, *Il Nuovo Cimento A* **11** (1998) 1243, https://link.springer.com/article/10.1007/BF03545792
39. S. Bhattacharyya, *Eur. Phys. J. A* **57** (2021) 164, and references therein, https://link.springer.com/article/10.1140/epja/s10050-021-00468-x
40. M. Sherif *et al.*, *IL Nuovo Cimento A* **109** (1996) 1135, and references therein, https://link.springer.com/article/10.1007/BF02798819
41. A. Abdelsalam *et al.*, *Chin. Phys. C* **37** (2013) 084001, https://iopscience.iop.org/article/10.1088/1674-1137/37/8/084001/pdf
42. A. Abdelsalam, *J. Korean Phys. Soc.* **67** (2015) 1150, https://link.springer.com/article/10.3938/jkps.67.1150
43. S. Kamel *et al.*, *Int. J. Mod. Phys. E* **30** (2021) 2150042, https://doi.org/10.1142/S0218301321500427
44. V. I. Bubnov *et al.*, *Z. Phys. A: At. Nucl.* **302** (1981) 133, https://link.springer.com/article/10.1007/BF01413043; D. Ghosh *et al.*, *Ann. Phys.* **45** (1988) 353, https://doi.org/10.1002/andp.19885000505.

45. R. A. Bodarenko *et al.*, *Yad. Fiz.* **38** (1983) 1483 (in Russian), https://inis.iaea.org/search/searchsinglerecord.aspx?recordsFor=SingleRecord&RN=16005000
46. N. N. Abd-Allah and M. Mohery, *Czech. J. Phys.* **51** (2001) 1189; ABGDDEKKLMRTTV Collab. (P. N. Andreeva *et al.*), *Sov. J. Nucl. Phys.* **45** (1987) 78.
47. B. P. Bannik *et al.*, *Czech. J. Phys. B* **31** (1981) 490, https://link.springer.com/article/10.1007/BF01596415
48. A. Dabrowska *et al.*, *Nucl. Phys. A* **693** (2001) 777, https://doi.org/10.1016/S0375-9474(01)00919-8
49. G. Q. Li *et al.*, *Z. Phys. A* **340** (1991) 271, https://link.springer.com/article/10.1007/BF01294675
50. S. Ahmad *et al.*, *Int. J. Mod. Phys. E* **18** (2009) 1929, https://doi.org/10.1142/S0218301309013968
51. S. Bhattacharyya, *Eur. Phys. J. Plus* **132** (2017) 229, and references therein, https://link.springer.com/article/10.1140/epjp/i2017-11539-0
52. M. S. El-Nagdy *et al.*, in *Proc. 2nd Conf. Nuclear and Particle Physics (NUPPAC'99)* Cairo, 13–17 November 1999, eds. M. N. H. Comsan and K. M. Hanna (ENPA, 2000), p. 467, https://www.osti.gov/etdeweb/biblio/20818335
53. A. Abdelsalam *et al.*, *Can. J. Phys.* **89** (2011) 261, https://cdnsciencepub.com/doi/abs/10.1139/P11-011
54. N. Marimuthu *et al.*, *DAE Symp. Nucl. Phys.* **63** (2018) 922, https://inspirehep.net/literature/1731339
55. U. Singh and K. Singh, *J. Korean Phys. Soc.* **76** (2020) 297, https://link.springer.com/article/10.3938/jkps.76.297
56. I. Segal *et al.*, *J. Phys. Conf. Ser.* **1690** (2020) 012107, https://iopscience.iop.org/article/10.1088/1742-6596/1690/1/012107/pdf
57. S. Bhattacharyya, *Int. J. Mod. Phys. E* **29** (2020), 2050020, https://doi.org/10.1142/S0218301320500202
58. H. H. Heckman *et al.*, *Phys. Rev. C* **17** (1978) 1651, https://doi.org/10.1103/PhysRevC.17.1651
59. EMU01 Collab. (M. I. Adamovich *et al.*), *Phys. Rev. Lett.* **62** (1989) 2801, https://journals.aps.org/prl/abstract/10.1103/PhysRevLett.62.2801
60. A. El-Naghy *et al.*, *J. Phys. G: Nucl. Phys.* **14** (1988) 1125, https://iopscience.iop.org/article/10.1088/0305-4616/14/8/015
61. A. Abdelsalam *et al.*, *Int. J. Mod. Phys. E* **23** (2014) 1450040, https://doi.org/10.1142/S0218301314500402
62. S. Gupta *et al.*, *Phys. Lett. B* **829** (2022) 137021, https://www.sciencedirect.com/science/article/pii/S0370269322001551
63. B. Alver *et al.*, *Phys. Rev. C* **94** (2016) 024903, https://arxiv.org/pdf/1511.07921.pdf
64. N. Burtebayev *et al.*, *Universe* **8** (2022) 67, https://doi.org/10.3390/universe8020067
65. M. Mohery *et al.*, *Int. J. Mod. Phys. E* **29** (2020) 2050063, https://doi.org/10.1142/S0218301320500639
66. H. Heiselberg, *Phys. Rep.* **351** (2001) 161, https://doi.org/10.1016/S0370-1573(00)00140-X
67. EMU01 Collab. (M. I. Adamovich *et al.*), *Phys. Lett. B* **223** (1989) 262.
68. A. Alexandrov *et al.*, *Nucl. Instrum. Methods Phys. Res. A* **776** (2015) 45.
69. EMU01 Collab. (M. I. Adamovich *et al.*), *J. Phys. G: Nucl. Part. Phys.* **22** (1996) 1469.
70. S. Bhattacharyya *et al.*, *Eur. Phys. J. Plus* **134** (2019) 37.